STAR Protocols

CellPress
OPEN ACCESS

Protocol

# Protocol for detecting and analyzing non-oscillatory traveling waves from high-spatiotemporal-resolution human electrophysiological recordings

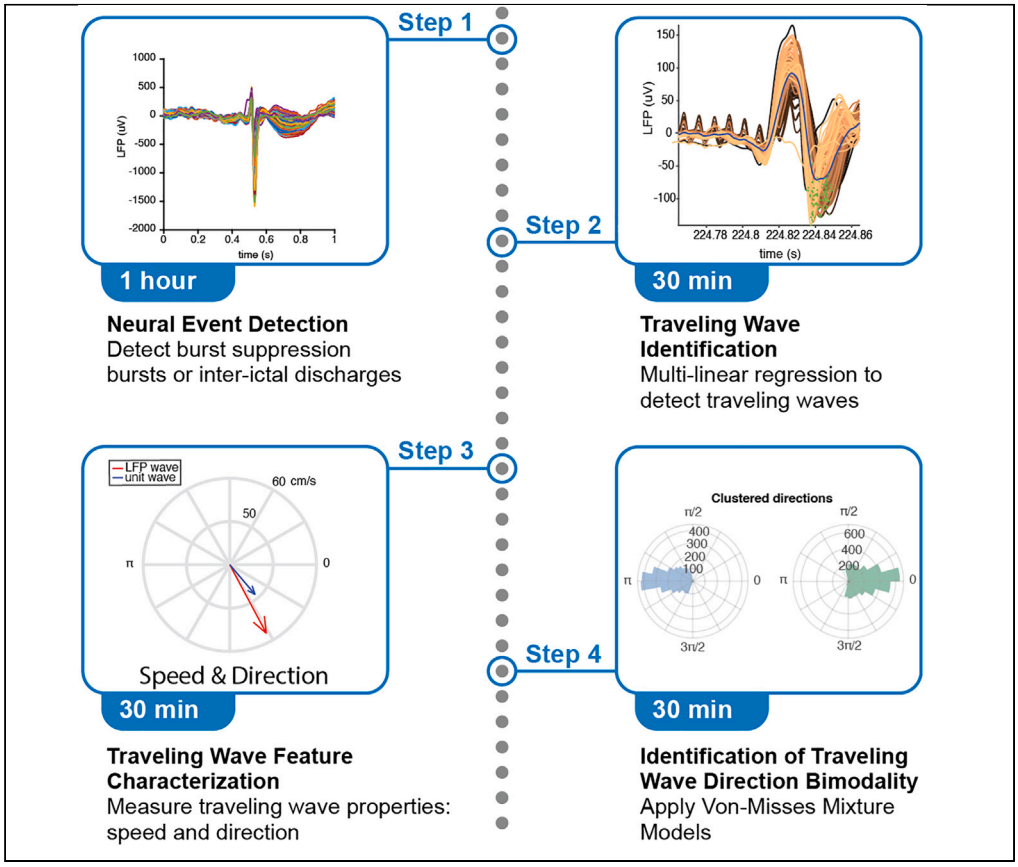


Innovations in electrophysiological recordings and computational analytic techniques enable high-resolution analysis of neural traveling waves. Here, we present a protocol for the detection and analysis of traveling waves from multi-day microelectrode array human electrophysiological recordings through a multi-linear regression statistical approach using point estimator data. We describe steps for traveling wave detection, feature characterization, and propagation pattern analysis. This protocol may improve our understanding of the coordination of neurons during non-oscillatory neural dynamics.

Publisher's note: Undertaking any experimental protocol requires adherence to local institutional guidelines for laboratory safety and ethics.

Veronica M. Zarr, Jyun-You Liou, Edward M. Merricks, ..., Catherine A. Schevon, John D. Rolston, Elliot H. Smith

veronica.zarr@utah.edu (V.M.Z.)
e.h.smith@utah.edu (E.H.S.)

## Highlights

Detect traveling waves using multi-linear regression statistical methodology

Characterize spatiotemporal features of traveling waves

Quantify propagation patterns of traveling waves

Zarr et al., STAR Protocols 6, 103659
March 21, 2025 
https://doi.org/10.1016/j.xpro.2025.103659

STAR Protocols

CellPress
OPEN ACCESS

Protocol

# Protocol for detecting and analyzing non-oscillatory traveling waves from high-spatiotemporal-resolution human electrophysiological recordings

Veronica M. Zarr,[1,12,*] Jyun-You Liou,[3] Edward M. Merricks,[2] Tyler S. Davis,[1] Kyle Thomson,[4] Bradley Greger,[5] Paul A. House,[6] Ronald G. Emerson,[7] Robert R. Goodman,[8] Guy M. McKhann II,[9] Sameer A. Sheth,[10] Catherine A. Schevon,[2] John D. Rolston,[11] and Elliot H. Smith[1,2,13,*]

[1]Neurosurgery Department, University of Utah, Salt Lake City, UT 84117, USA
[2]Department of Neurology, Columbia University, New York, NY 10032, USA
[3]Department of Anesthesiology, Weill Cornell Medicine, New York, NY 10065, USA
[4]Department of Pharmacology & Toxicology, University of Utah, Salt Lake City, UT 84117, USA
[5]School of Biological & Health Systems Engineering, Arizona State University, Tempe, AZ 85281, USA
[6]Neurosurgical Associates, LLC, Murray, UT 84107, USA
[7]Hospital for Special Surgery, New York, NY 10021, USA
[8]Lenox Hill Hospital, New York, NY 10075, USA
[9]Department of Neurological Surgery, Columbia University, New York, NY 10032, USA
[10]Department of Neurosurgery, Baylor College of Medicine, Houston, TX 77030, USA
[11]Brigham & Women's Hospital, Harvard Medical School, Boston, MA 02115, USA
[12]Technical contact
[13]Lead contact
*Correspondence: veronica.zarr@utah.edu (V.M.Z.), e.h.smith@utah.edu (E.H.S.)
https://doi.org/10.1016/j.xpro.2025.103659

## SUMMARY

**Innovations in electrophysiological recordings and computational analytic techniques enable high-resolution analysis of neural traveling waves. Here, we present a protocol for the detection and analysis of traveling waves from multi-day microelectrode array human electrophysiological recordings through a multi-linear regression statistical approach using point estimator data. We describe steps for traveling wave detection, feature characterization, and propagation pattern analysis. This protocol may improve our understanding of the coordination of neurons during non-oscillatory neural dynamics.**

**For complete details on the use and execution of this protocol, please refer to Smith et al.[1]**

## BEFORE YOU BEGIN

In this work, we illustrate how to employ traveling wave analysis techniques in microelectrode array recordings to understand their role in physiological and pathological non-oscillatory neural events such as interictal discharges (IEDs) and anesthesia induced bursts. Recent studies using high spatiotemporal resolution sensors have revealed the importance of propagating brain activity known as traveling waves, in controlling neuronal communication and activation.[2] Innovations in electrophysiological recording and computational analytic methodologies have enabled the high-resolution measurement and analysis of distributed neural activity, providing new approaches for investigating their functional properties.[3,4] In this protocol we describe a multi-linear regression based statistical approach used in prior studies[1,3,5] to capture and analyze traveling waves in the human brain amidst non-oscillatory neuronal signals in Utah microelectrode array (UMA) recordings.

  

Researchers have detected and analyzed traveling waves using various methods including partitioning UMAs into quadrants,[6] positive and negative centers of mass,[5] multilateration source localization,[7–9] generalized phase[10] or using an oscillatory phase-based approach.[4,11,12] Phase-based approaches are designed to study oscillatory activity, which may limit their use for the full repertoire of human neural activity.[4] Neural activity such as interictal discharges, evoked potentials and anesthesia-induced burst-suppression are all non-oscillatory, potentially violating the assumptions of phase-based methods.

Our approach overcomes several challenges for analyzing these waves in the human brain. First, we describe our approach for detecting traveling waves across the microelectrode array in non-oscillatory neural activity using point estimators. We then describe methods to detect and analyze the spatiotemporal features of these detected traveling waves. Finally, we describe several features of the detected traveling waves and how they are related to human neural function. Our approach is rigorous and can be used to detect and characterize the spatiotemporal propagation patterns of traveling waves in a diversity of non-oscillatory neural events. A step-by-step visual demonstration of the multi-linear regression statistical methodology to detect traveling waves in non-oscillatory neural activity has been provided in this protocol.

> *Note:* Please note that the code for implementing this protocol on your data is available in the article's GitHub repository, which can be accessed here. Additionally, a sample dataset is provided in the repository to help you verify the method step-by-step. It is important to note that the code in this protocol and the corresponding GitHub repository is designed for use with MATLAB. However, we provide a comprehensive explanation of the method, which can be adapted to other programming languages like Python with necessary syntax modifications. Our approach is flexible in that it may be applied to other recording modalities such as scalp EEG and MEG recordings as well as recordings from animal models.[13]

## Institutional permissions

Human subject participation for our study (Smith et al., 2022) was approved by the University of Utah and Columbia University Medical Center Institutional Review Boards. Informed consent was obtained from all study participants prior to the implantation of the research UMA and clinical electrocorticography (ECoG) electrodes used to identify seizure foci.

## Preparation: Install MATLAB and MATLAB toolboxes

Timing: <1 min

1. Download MATLAB2022B or a more recent version from https://matlab.mathworks.com/.
   a. To perform parallel computations on multiple clusters, install the parallel processing toolbox from https://www.mathworks.com/products/parallel-computing.html.
   b. To perform signal processing and analysis, install the signal processing toolbox from https://www.mathworks.com/products/signal.html.
   c. To apply mixtures of von Mises distributions to perform probabilistic modeling of circular data, install the fitmvmdist MATLAB toolbox from (https://github.com/chrschy/mvmdist).

## Data collection

We present this protocol based on a study of ECoG and UMA data from 10 adult neurosurgical patients.[1] We provide the pre-processed dataset of IED detections across the UMA (Blackrock Microsystems Inc, Salt Lake City, UT) implanted in 10 participants (see key resources table). The complete surgical protocol for UMA implantation can be found in House et al.[14] ECoG and UMAs are implanted in the predicted seizure onset zone, based on preoperative electroencephalographic studies, neuroimaging, and intraoperative ECoG.[15] UMAs were connected on the first day of the patient's hospital stays, and electrophysiological data were recorded throughout the duration of the

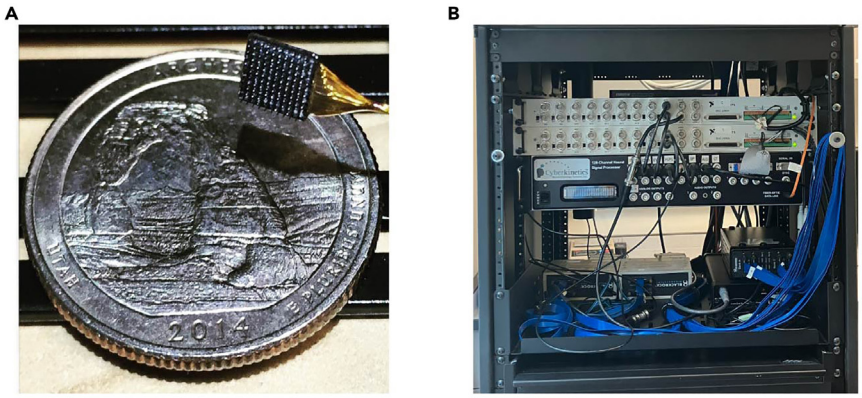


**Figure 1. Setup for Utah array recording**

(A) "Utah" style microelectrode array (top right; UMA) next to a US quarter dollar for scale. The UMA has 96 microelectrodes, configured in a 10 by 10 grid with 400 μm inter-electrode distance and 1 mm electrode length. (B) Blackrock neural signal processing system under National Instruments breakout boards and above splitter boxes for the neurostimulator and the amplifier.

participants' neuromonitoring sessions, including during anesthesia induction for two patients discussed here that were not included in Smith et al. The fine spatiotemporal resolution of the UMA enables the discernment of temporal delays over submillimeter distances providing excellent characterization of traveling wave properties.[16,17]

A neural signal processing system (Blackrock Microsystems, Salt Lake City, UT) was used to acquire direct brain activity recordings at 30 kilosamples per second, hardware filtered between 0.3 Hz and 7.5 kHz and pseudodifferentially amplified by 10. Electrophysiological data were recorded onto mirrored hard drive arrays and then transferred in the NS5 file format onto two HIPAA-compatible secure servers in New York City and Salt Lake City. The data collection equipment setup is shown in Figure 1.

## Data pre-processing

The purpose of this section is to pre-process the data. Prepare the dataset for traveling wave analyses by detecting local field potential (LFP) and multiunit action potential (MUA) data from each microelectrode.

2. Apply a bandpass filter to each channel, segregating the frequency ranges from 0.3 and 3 kHz for MUA, and below 300 Hz for LFP.

   ***Note:*** Figure 2 recordings were obtained using a sampling frequency of 30,000 Hz (30 kHz). Figure 2A shows an example filtered broadband LFP signal recording containing all signals from the 96 electrodes of the UMA.

3. The next step is to filter and normalize each channel: for each channel in the data matrix use "filtfilt" matlab function, to filter each channel and then subtract the mean from the filtered signal to normalize it.
4. Calculate the threshold for detecting spikes based on the root mean square (RMS) of the filtered signal.
   a. Set the threshold at 4 times the negative RMS value.

   ***Note:*** This negative threshold helps in identifying the downward spikes (or minima) in high frequency events that most likely represent action potentials.

5. Detect spikes in the filtered MUA band less than 4 times its root mean square and retain the timestamps of the detected action potentials for subsequent analysis.

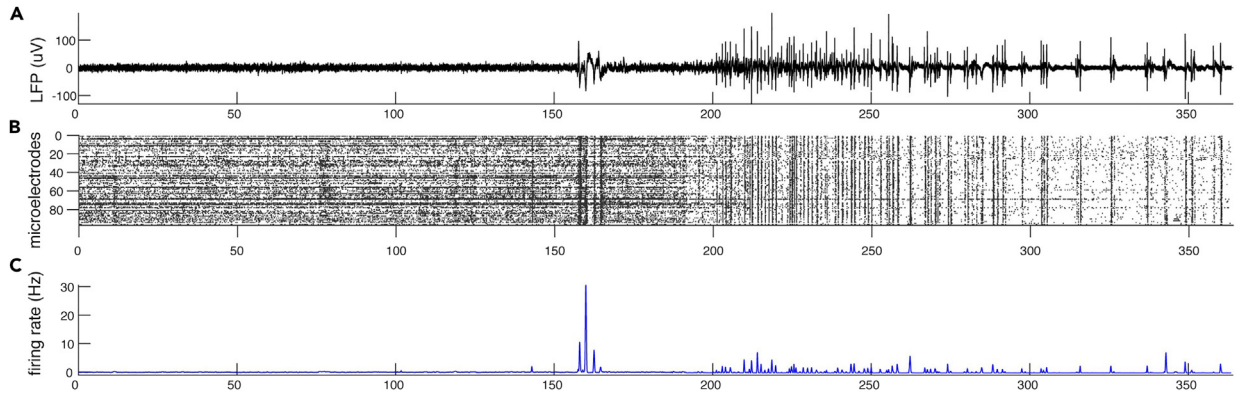


**Figure 2. Utah array recording**

An example pre-processed Utah array recording from the middle temporal gyrus of a neurosurgical patient as they lost consciousness under propofol anesthesia.

(A) Broadband mean LFP signal averaged across channels on the UMA.

(B) Raster plot of multi-unit event times across the UMA.

(C) Mean multi-unit firing rate across the UMA.

a. To detect spikes, use the "find_inflections" matlab function[18] to detect the minima (inflection points) in the filtered signal.

*Note:* The function then selects the timestamps of the minima that fall below the threshold. A representative raster plot of MUA event times is shown in Figure 2B.

6. To estimate a continuous firing rate for the MUA recorded on each microelectrode, we applied a Peri-Stimulus Time Histogram (PSTH) using the "Psth" matlab function.[19]
   a. Specify the bin size and Gaussian kernel window to match the duration of the signal of interest.

*Note:* The MUA spike times for each channel, as displayed in the raster plot in Figure 2B, were convolved with a Gaussian kernel using the "smoothdata" matlab function.[20] A bin size of 25 ms and a Gaussian smoothing window of 10 bins were applied, resulting in a 250 ms smoothing window that produced the mean firing rate shown in Figure 2C.

## KEY RESOURCES TABLE

| REAGENT or RESOURCE | SOURCE | IDENTIFIER |
|---|---|---|
| Deposited data | | |
| Raw and analyzed data | Smith et al.[1] | https://osf.io/zhk24/ |
| Participant information (age and gender) | Smith et al.[1] | Appendix 1—table 1 |
| Code repository | Smith et al.[1] | https://github.com/elliothsmith/IEDs<br>https://github.com/neurosmiths/Data-and-Code-for-STAR-Protocols |
| Software and algorithms | | |
| MATLAB 2021b | The MathWorks, Inc | https://de.mathworks.com/products/matlab.html |
| Circular statistics toollbox | Berens[21] | https://github.com/circstat/circstat-matlab |
| fitmvmdist | Schymura C, 2016[22] | https://github.com/chrschy/mvmdist |
| hrtest | Cloherty, 2020[23] | https://github.com/cnuahs/hermans-rasson |
| Other | | |
| Blackrock recording system | Blackrock Neurotech | https://blackrockneurotech.com/research/products/ |
| UMA; 10 × 10 microelectrodes in 4 × 4 mm grid, penetrating 1 mm | Blackrock Neurotech | https://blackrockneurotech.com/research/products/ |

**Table 1. Computational resources used in this study**

| CPU information | Value |
|---|---|
| RAM | 16 GB |
| Cores | 6 |
| Processor Speed | 1.1 GHz |

## MATERIALS AND EQUIPMENT

A minimum of 16 GB local memory and 1.1 GHz processing speed is recommended, please refer to Table 1 for the computational resources used in this study.

## STEP-BY-STEP METHOD DETAILS

This section details the process of traveling wave detection, spatiotemporal feature characterization and wave propagation pattern analysis. We also describe steps for signal artifact removal.

### Data cleaning and artifact removal

Timing: <1 min

Various types of artifacts can appear on UMA recordings. In this section we briefly discuss how to remove several of the most common and salient types of artifacts.

*Note:* The most straightforward method of artifact removal is to trim aspects of the data that are clearly artifactual from visual inspection. There are other algorithmic methods for artifact removal that could be employed in this data. Examples of such methods have been detailed in other publications and are reviewed here.[5,14,24,25]

1. Remove artifactually large IEDs by excluding IEDs with mean amplitudes across channels that surpass 2x the interquartile range of the channel-averaged voltage range distribution across detected IEDs.

*Note:* Artifacts across all channels in a circumscribed time period: For example, the large LFP deflections associated with the highest MUA firing rates at approximately 160 s in Figure 2 might be a movement or muscle artifact. These time points could be manually trimmed from the raw data in order to avoid propagating through both the LFP and MUA wave measurements. From our experience, such artifactual bursts do not propagate, nor meet the criteria to be classified as traveling waves, so will also be removed at the traveling wave classification stage.

*Note:* Artifacts within particular channels: For example, some of the firing in the raster plot in Figure 2, might be artifactually high. Perhaps there is high frequency noise on these channels that is surpassing the MUA threshold. These channels could also be removed based on visual inspection. Another method for finding broken channels in UMA data is to cluster the channels in principal component space. Broken channels or other channels with excessive line noise tend to cluster together and can be isolated for removal from the dataset.

### Neural event detection

Timing: <1 min

In this section we describe the procedure for detecting IEDs, as used in Smith et al. (2022), but these steps can generally be used to characterize the spatiotemporal propagation of anesthesia bursts, or various other non-oscillatory events. In such cases, some of the numbers specified below may vary.

*Note:* Our approach for traveling wave detection has been applied to measure traveling waves in non-oscillatory neural activity obtained via direct brain recordings from UMAs implanted in adult patients undergoing surgery for intractable epilepsy.[1] Many previous studies of traveling waves in human brain recordings have detected and analyzed traveling waves based on the spatial gradient of phases and by using a circular-linear regression approach.[4] These approaches assume that neural activity is oscillatory. However, much neural activity is non-oscillatory. Therefore, alternative methods for measuring traveling waves would be preferable to study traveling activity in non-oscillatory neural events as well as to prevent artifacts introduced by narrow-band filtering such as waveform distortion. Notably, traveling waves may be detected from a range of low frequency phases by identifying phase offsets across electrodes in a generalized phase computed from low frequency LFP activity (5–40 Hz).[10] We found this approach to generate similar results to the point estimator method in recent work examining traveling waves evoked from electrical stimulation.[26] This approach consists of two primary steps: the first step consists of identification of the non-oscillatory neural event of interest i.e., an ictal or interictal discharge or bursting during anesthesia induced burst suppression. The second step consists of regressing the timing of LFP features or neuronal firing rates against the dimensions of the recording array.

2. Signal pre-processing.
   a. Resample the data to 400 samples per second, then apply a fourth-order Butterworth filter to each channel to zero-phase the signal and isolate activity within the beta frequency range (20–40 Hz).
   b. Smooth the absolute value of the amplitude of the filtered beta signal to reduce noise and improve peak detection sensitivity.
3. IED Detection.
   a. Use the "findpeaks" matlab function[27] to detect peaks in the smoothed, beta-filtered signal.

⚠ CRITICAL: Operationally define interictal epileptiform discharges (IEDs) as high-amplitude peaks or bursts of beta-range (20–40 Hz) LFP power observed across at least 10 microelectrodes.

*Note:* Smith et al. (2022) developed an algorithm to detect IEDs across a microelectrode array. For Matlab implementation please refer to the code repository section of the key resources table, where you can find the IED detection algorithm.[1] This algorithm identifies periods of abnormally high beta power occurring simultaneously across at least 10 microelectrodes.

   b. Set the minimum peak height criterion to identify peaks that exceed eight times the standard deviation of the beta power across the recording, effectively differentiating IEDs from background activity.
   c. Record timestamps for identified peaks that occur within the same 250 ms window across at least 10 electrodes, marking these as potential IEDs.
   d. Remove redundant detections defined as peaks occurring within 250 ms of a preceding detection on the same channel by retaining only the first detected peak.
4. Apply smoothing window. Once IEDs are identified (Figure 3D), follow these steps to mark the time to voltage minima for each channel:
   a. Apply a smoothing window to the LFP data to generate the smoothed data that will be used to identify the local and absolute minima.

*Note:* The smoothing window size is calculated as the sampling frequency (Fs) divided by the binFactor. This step ensures the robustness of subsequent analyses. A smoothing window size of 1 second was used in Figure 3E.

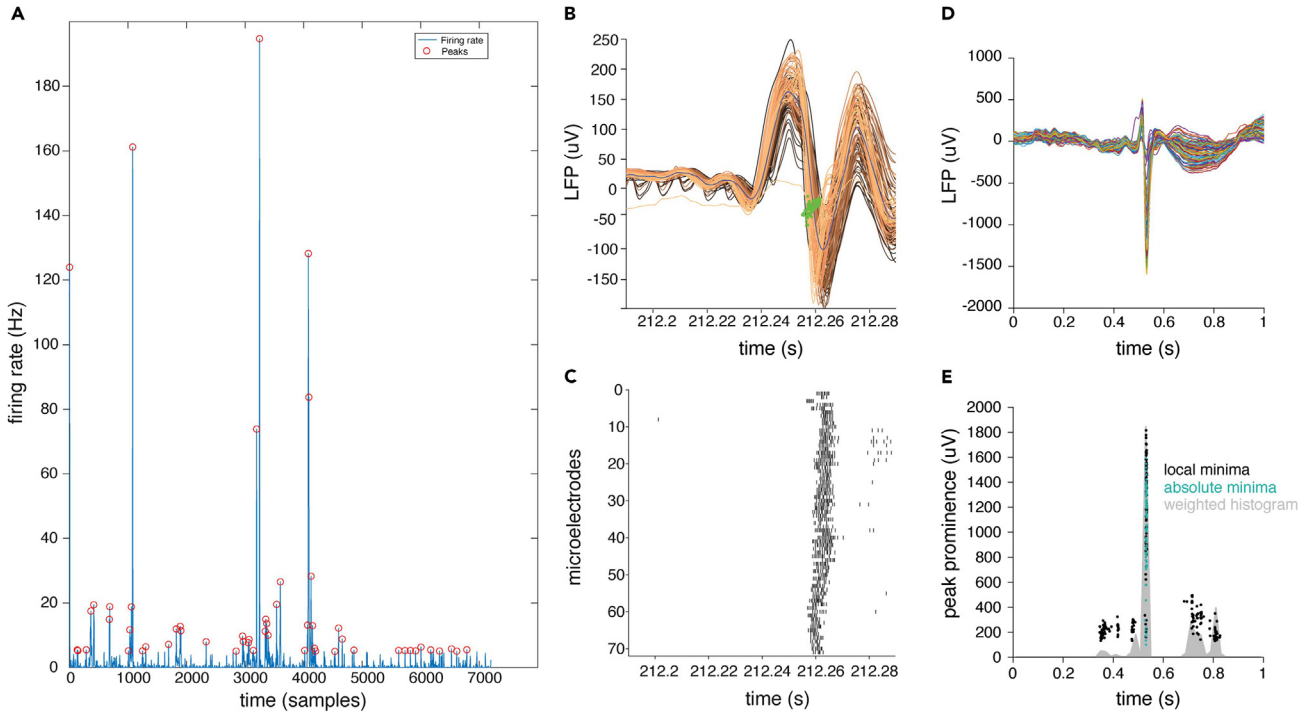


**Figure 3. Neural event detection analysis**

(A) Anesthesia bursts (red circle) detected from the peak of the firing rate (blue) obtained by convolving the MUA firing by a Gaussian kernel.

(B) LFP voltages during a representative example anesthesia burst recorded across all channels of the UMA. LFP voltages are colored by time to the signal minimum; green dots indicate time points of maximal descent.

(C) MUA firing during a representative example anesthesia burst recorded across all channels of the UMA.

(D) LFP voltages of a representative example of an IED recorded across all channels of the UMA. Colored by microelectrode channel.

(E) Timing of voltage extrema detected by local minima convolved with a Heaviside function to create a weighted histogram displaying scatter plot of IED extrema over time, black dots show local minima and green dots show absolute minima, gray shows weighted histogram of points used to define the time bin used for extrema detection.

5. Detect local and absolute voltage minima.
   a. For each channel, identify the local voltage minima using the islocalmin function.

   *Note:* This step ensures that only significant minima are captured by applying a prominence threshold (MinProminence) based on the median of the standard deviations of the signal across channels.

   b. Additionally, compute the absolute minima for each channel using the min function.
6. Bin local voltage minima:
   a. For each channel, bin local voltage minima within a time window around each IED event.

   *Note:* The time window is defined by the edges array. An edges array of 0:0.02:1 was used in Figure 3E, which spans 1 second and is divided into 50 bins to create a bin width of 0.02 seconds. This 1-second time window is separate from the smoothing window used in the smoothing process described in step a.

7. Convolve the binned data histogram with a modified Heaviside function (weighting function) to generate a weighted histogram of the local minima, as shown in Figure 3E.

*Note:* Here, n represents the time base for the convolution process. This modified Heaviside function emphasizes the central portion of the time window, giving higher weight to bins closer to the center and lower weight to those at the edges.

$$H(t) = \begin{cases} 0, & 0 \geq n < 0.4 \\ 10t, & 0.4 \geq n < 0.5 \\ -t, & 0.5 \geq n < 1 \end{cases}$$

8. Identify absolute minima. After applying the modified Heaviside function to the histogram, identify the bin with the highest weighted count.

*Note:* Locate the absolute minima of V(c,t) within the bin containing the highest number of local minima. This method is more robust to noisy bursts or polyspikes, but this bin often also has the most detected absolute minima.

9. To identify bursts during anesthesia induced burst suppression, operationally define a burst as the peak of the firing rate obtained from convolving MUA firing times with a Gaussian Kernel during data pre-processing.

*Note:* For Matlab implementation please refer to the code repository section of the key resources table, where you can find the burst detection algorithm and example UMA recording during propofol-induced loss of consciousness.

   a. Find peaks in the firing rate with the "findpeaks" matlab function[27] utilize the minimum peak prominence criteria to detect isolated peaks in the firing rate.

*Note:* After detecting the peak firing time, record the timestamps or time indices of the detected peaks or neural bursts for subsequent analysis. Figure 3A visualizes the outcome of this step showing the peaks detected from the convolved MUA firing times.

   b. Determine the time window to loop through the peaks for traveling wave analysis.

*Note:* Use half of the median minimum difference in time between bursts to calculate the time window around each detected peak or burst. Use this time window to record and analyze the LFP signal and unit firing that coincides with each detected burst. Figure 3B illustrates an example recording containing the LFP signals and Figure 3C illustrates the corresponding unit firing across the UMA during a burst using a 100 ms time window.

10. Once the neural events have been detected, extract the neural event timings for subsequent traveling wave detection analysis.
   a. Loop over each LFP channel and extract the LFP point estimator of choice such as maximal descent (steepest negative slope) or the negative peak (largest negative amplitude) in the LFP signal. For the MUA data, loop over each MUA channel and extract the MUA timings.
   b. Store the neural event timings corresponding to these features for further use, such as fitting a multilinear regression to the neural event timings for traveling wave detection.

*Note:* Several features of the neural signals may be used to calculate the neural event timings; multi-unit spike timings as well as field potential-based measures of neural events (negative peak and point of maximal descent), visualized in Figure 4. Liou et al. found that negative peak and maximal descent were the most computationally efficient and robust markers for

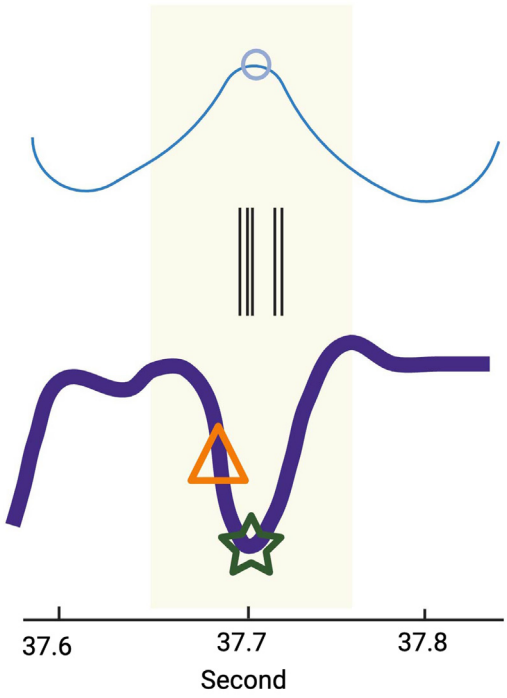


**Figure 4. Schematic of MUA and LFP point estimators**

Visualization of neural event timing methods using data from a single channel. After detecting the peak firing time (circle), all electrical activity within 50 ms of the peak is attributed to the neural event (light yellow). Multiunit spikes (black), LFP (purple), timing of the negative peak (star) and maximal descent (triangle). Created in BioRender. Zarr, V. (2024).

calculating traveling wave speed, when compared with other more computationally expensive point estimators such as LFP cross-correlation and high gamma power.[3] Phase based methods would likely fall between these two groups of methods in computational efficiency.

*Note:* The LFP negative peak or voltage minima timing is defined as the minimum value in the time window assigned to each neural event. The time of maximal descent is defined as $\text{argmin}_t \frac{\Delta L(t)}{\Delta t}$, where $L$ is LFP voltage and $t$ is time. The maximal descent reflects the point at which the downward deflection is steepest and best corresponds to the median timing of single neuron firing during epileptiform discharges.[3,5]

## Traveling wave detection

Timing: <1 min

This section describes the process for traveling wave classification from multi-unit action potentials and LFP which consists of regressing the timing of LFP features or neuronal firing against the dimensions of the microelectrode array.

*Note:* After identifying a non-oscillatory neural event such as an anesthesia induced burst or IED, which will determine the time window for analysis, the next step in our framework is to identify traveling waves that propagate within that time window.

11. Once neural event timings have been calculated as detailed in the previous section, the first step to detect traveling waves in neuronal signals is to fit an ordinary multilinear regression plane to the neural event timings across the UMA.

*Note:* Our approach operationally defines traveling waves as regression models with slopes that significantly differ from zero.

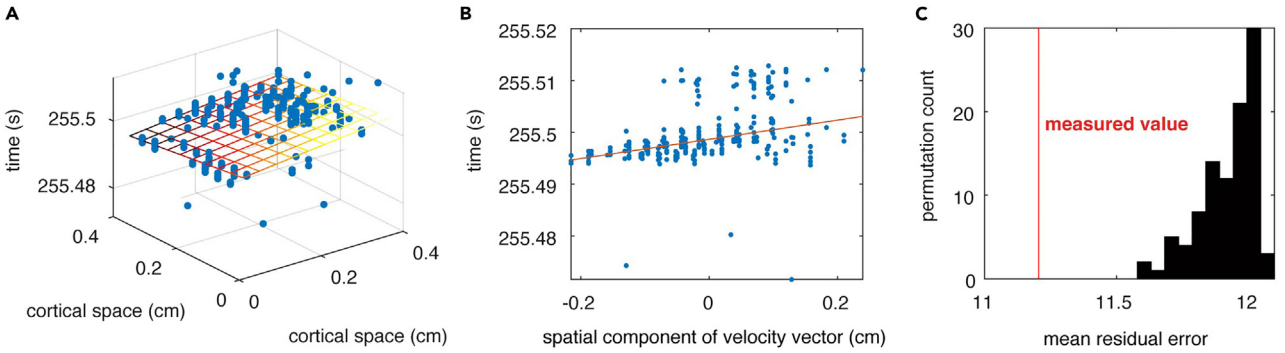


**Figure 5. Wave detection analysis**

(A) Visualization of 3D scatterplot of voltage minima timings fitted by best fit plane from the multilinear regression model, regularized via minimization of square error. Propagation axis is colored by activation sequence (blue to yellow).

(B) The projection of voltage minima timings along the regression plane's gradient (propagation axis).

(C) Visualization of permutation test used to identify traveling waves. Red: true residual absolute deviation. Black: residual absolute deviations from spatially shuffled data.

a. Treat each neural event as a 3D data point ($P_x$, $P_y$, t). $P_x$ and $P_y$ represent the two-dimensional spatial locations of the electrodes across the microelectrode array plane and t represents the neural event times.

*Note:* This model has the following structure,

$$\beta = (P'P)^{-1} P'T$$

where each row of the matrix P contains the spatial location of the recording microelectrode and the column vector T contains the neural event timings.[28] see Figure 5A for three-dimensional visualization of the non-flat slope of the linear regression plane fitted to LFP voltage minima timings, indicating the presence of sequential neuronal activation across recording sites. Figure 5B visualizes burst timings regressed against the single spatial dimension of distance between each electrode.

*Note:* Projecting the three-dimensional spatial locations into two dimensions assists with better visualization and interpretation of the traveling wave and its features. The projection takes the multidimensional 3D spatial data (in this case, the x- and y-coordinates of the recording electrodes) and "flattens" it along a single axis, aligned with the estimated traveling wave velocity vector. This allows for a 2D visualization where the x-axis represents the position of electrodes projected onto the wave's direction and the y-axis represents the neural event timings, so that if there is a traveling wave, you should see a strong relationship between neural event timings and electrode positions when plotted along the wave's direction.

b. Estimate the model βs by minimizing either the least absolute deviation or the squared error in the multivariate linear regression equation via L1 or L2 regularization respectively.

*Note:* There are two regularization methods that can be used for this step: L1 regularization which minimizes the least absolute deviation and is used to minimize the impact of outliers on slope estimation and L2 regularization which minimizes the squared error in the multivariate linear regression. The regression model applied to each neural event should produce three coefficients, characterizing the best-fit plane of the neural event timings across the bed of the microelectrode array.

12. To test for the statistical significance of a traveling wave, operationally define a traveling wave as sequential neuronal activation as measured by regression slopes significantly different from zero.

*Note:* Significant traveling waves will be simultaneously operationally defined and controlled for false positives and multiple hypothesis testing using non-parametric permutation testing against a null distribution of models with shuffled electrode locations (Figure 5).

a. Use an F-test with $\alpha = 0.05$ to reject the null hypothesis that the MUA firing and LFP point estimator timings occur simultaneously, as measured by the non-flat slope of the linear regression model, i.e., $\beta 1 = \beta 2 = 0$.

*Note:* A traveling wave can be described as the sequential multi-unit firing or neural event timings across recording sites, versus the null hypothesis that multiunit spikes or neural event timings occur simultaneously, or without a consistent spatial pattern. We can operationally define a traveling wave as a sequential neuronal firing or activation in the linear regression of time (MUA timings, LFP maximal descent timings) across space (microelectrode array footprint) and perform an F-test against the null hypothesis of zero slope for each detected non-oscillatory neural event, i.e. $\beta 1 = \beta 2 = 0$. This permutation procedure controls for false discoveries and ensures the true pattern of propagation is unlikely to occur by chance. To perform this task, we use linear regression which models the relation between electrode position and neural event timings (Figure 5).

b. Perform a permutation test against a distribution of 500 spatially permuted neural event timings.

*Note:* Traveling wave model significance is assessed via an F-test against a permutation distribution of 500 spatially shuffled LFP or firing times. Significance is assessed by whether the true test statistic is greater than 95% of the test statistics from a null distribution of spatially shuffled neural event timings.

*Note:* Figure 5C visualizes the permutation test, showing a histogram of the residual errors obtained from the shuffled data. Each value in this distribution corresponds to a residual error calculated when the spatial positions were randomly shuffled and the model was refit. The shuffled distribution corresponds to the distribution of test statistics under the null hypothesis (the absence of a traveling wave). The red vertical line shows the residual error from the non-shuffled true data, and its position relative to the distribution of shuffled residuals indicating the model's significance. If the actual residual is much lower than most of the shuffled residuals as it is in Figure 5C, it suggests that the model fit is significantly better than expected by chance, so that we can say with high confidence that a traveling wave has been detected.

*Note:* An advantage of this approach is that it prevents artifacts introduced by narrow-band filtering such as waveform distortion as it enables the detection of traveling waves in broad-band LFP and MUA firing activity.

### Traveling wave feature characterization

Timing: <1 min

Once traveling waves have been identified, we can characterize their spatiotemporal features. This section shows how to describe the features of traveling waves, providing a tool for characterizing the spatiotemporal coordination of neuronal activity underlying different brain states.

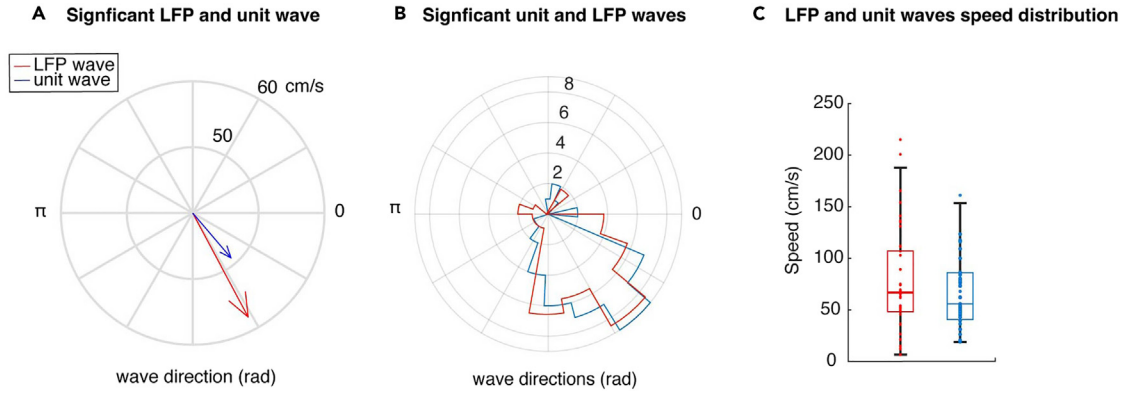


**Figure 6. Wave feature characterization**

(A) Quiver plot visualizing the speed and direction for a single LFP and unit wave regularized via least squares regression.

(B) Polar histogram showcasing all LFP and unit wave directions for a patient regularized via least squares regression.

(C) Boxplot showcasing the speeds for all LFP and unit waves for a patient regularized via least squares regression.

***Note:*** Neural traveling waves have been shown to be functionally relevant in cognition, disease and behavior.[1,2,29,30] Specifically, traveling wave properties such as direction and speed have been shown to be involved in normal, pathological and pharmacologically altered brain states such as sleep,[30,31] seizure[5,32,33] and medically induced loss of consciousness.[6,34–36] Additionally, traveling wave properties have been shown to be functionally relevant in memory,[11,12,31,37] motor and speech behaviors[38,39] and vision.[40,41]

13. Obtain the wave velocity by taking the pseudoinverse of the first two multilinear regression coefficients, $\widehat{\beta}, \widehat{V} = (pinv([\widehat{\beta} = \widehat{\beta}_1, \widehat{\beta}_2])$.

***Note:*** The multilinear regression model described in the previous section provides a very useful quantitative tool for measuring the spatiotemporal properties of the traveling waves. The three coefficients from the regression can be used to calculate all the key features of the traveling wave. For example, the wave propagation speed is obtained from the slope of the linear model. Other features of the traveling wave such as the wave direction may also be derived from these parameters.

***Note:*** From the velocity vector, both speed and direction can be described. Figure 6A visualizes the outcome of this step as a compass plot; directional information is apparent in the direction of the velocity vector visually represented as the arrows in the compass plot and speed is visualized by the arrow length indicating the magnitude of the velocity vector.

14. Obtain the traveling wave direction by examining the gradient direction of the regression plane, direction = $\tan^{-1}(pinv([\beta_1, \beta_2])$.

***Note:*** Figure 6B shows the distributions of burst LFP and MUA traveling waves as a polar histogram.

***Note:*** The bimodality analysis section describes how to derive a quantitative measure of direction by applying von Mises Mixture models (vMM) to the distributions of traveling wave directions.

15. Derive traveling wave speed from each significant model's slope by taking the magnitude of the model's gradient norm as described in detail in Liou et al.[3]
    a. Calculate the traveling wave speed by taking the L2 norm of the velocity vector, $\widehat{S} = \| \widehat{V} \|$ .

*Note:* The length of the vectors in the compass plot depicts the traveling wave speeds for MUA and LFP signals during a single burst. Figure 6C displays the speeds for all LFP and MUA burst traveling waves in a boxplot.

b. Test speed differences across participants or conditions by using a two-way Kruskal-Wallis Test.
   i. Utilize a significance threshold of 0.05 and conduct post-hoc pairwise comparisons using Dunn's test.

*Note:* Smith et al. (2022) used a 10-level participant factor (one level for each participant) and a signal factor with the two levels corresponding to speed measurements obtained from MUA and LFP signals. Permutation tests against shuffled categories would also be appropriate for one- or two- sample tests.

### Bimodality analysis

Timing: 1 h

This section describes how to determine whether the distributions of traveling wave directions deviate from a uniform circular distribution by applying von Mises Mixture models (vMM) to the distributions of traveling wave directions.

*Note:* Having determined the direction of the detected traveling waves, we can further characterize the spatiotemporal propagation pattern of the waves to understand whether they have a predominant propagation direction. To characterize the propagation patterns of the detected waves, it is necessary to first quantify their spatial features.

*Note:* vMM analysis was used in Smith et al. to characterize the propagation patterns of IEDs relative to seizures and found that IEDs are bidirectionally propagating traveling waves with predominant, consistent directions of travel that could be used to predict seizure directions; potentially providing a novel biomarker for localizing the epileptic network.[1]

*Note:* vMMs are analogs of Gaussian Mixture models in polar coordinates. The vMM analysis indicates whether two unimodal distributions provide a better fit for traveling wave distributions than one unimodal distribution indicating a bimodal or bidirectional propagation pattern. Figure 7 visualizes the outcomes of each step for this section.

16. To quantify the propagation patterns of traveling waves, fit a von Mises Mixture Model (vMM) to the overall distribution of traveling wave directions.
    a. Use the "fitmvmdist" MATLAB function[21] to apply the vMM to the direction distributions.
    b. Apply MATLAB "cluster" function to the overall neural event direction distributions to derive two-component vMM distributions.
    c. Set the upper limit for hypothesized clusters ($h$) at two for distributions exhibiting two or fewer observed modes.
    d. Evaluate the distributions defined by $\mu_h$ and $\kappa_h$ using the DTS statistic, rather than the Kuiper test, to determine whether the vMM sub-distributions or the overall distribution provide a better fit.

*Note:* For sample sizes larger than 20, if the Kuiper test is still utilized, it is crucial to apply the scaled test statistic ($\sqrt{nV_n}$) rather than the traditional $V_n = D^+ + D^-$ formula to ensure proper normalization.

    e. Calculate $\mu_h$, $\kappa_h$, and $\theta_h$ for both the overall and vMM sub-distributions.

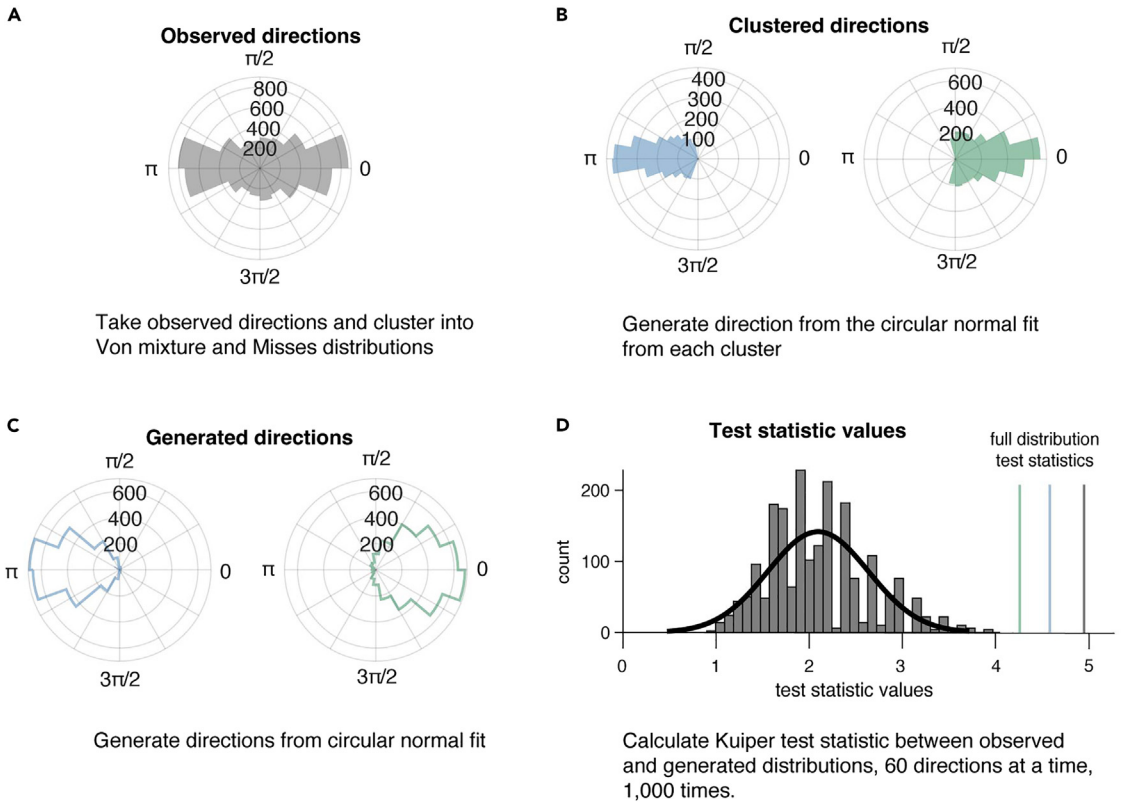


**Figure 7. Bimodality analysis**

(A) A polar histogram showing an example IED distribution for one participant.

(B) VMM clustered distributions of angles from the distribution shown in (A).

(C) Idealized distributions of the same number of directions in each sub-distribution shown in B, sampled from circular normal distributions with the same parameters as the clustered distributions shown in B.

(D) Visualization of the permutation test, showing the distribution of Kuiper test statistics comparing subsamples of angles from real IED distributions and circular normal distributions with the same parameters. The black line indicates the Gaussian fit to the distribution and colored lines represent the test statistics from the true data distributions.

*Note:* Each vMM cluster should yield three parameters for each cluster, such that $h$ is less than or equal to 2. These parameters consist of the sub-distribution means ($\mu_h$), concentration parameters ($\kappa_h$), and probability densities ($\theta_h$).

f. Compare the empirical distribution of 60 randomly sampled neural event directions to theoretical circular normal distributions derived from $\mu_h$ and $\kappa_h$ from both the overall distribution and the vMM sub-distributions using the DTS statistic.

g. Generate a permutation distribution by repeating the process 1,000 times.

*Note:* This distribution is used to measure differences between randomly sampled traveling wave angles and the theoretical circular distributions defined by both the overall distribution and the vMM sub-distributions.

h. Define the circular bimodality index as the minimum difference between the DTS test statistic for the overall distribution and for each vMM sub-distribution.

*Note:* Positive bimodality index values suggest that overall traveling wave distributions propagate bidirectionally as they are more accurately represented by two von Mises

sub-distributions, while negative bimodality index values suggest that overall traveling distributions are best described as a single von Mises distribution. A bimodality index close to zero, indicates a uniform direction distribution. The MATLAB functions for creating these classifications can be found in the online code repository, accessible through the key resources table.

*Note:* The original analysis employed the Kuiper test to evaluate traveling wave direction distributions. However, recent statistical literature has highlighted several limitations of this test, particularly when dealing with large sample sizes or non-normal distributions. Specifically, for sample sizes larger than 20, the traditional test statistic $V_n = D^+ + D^-$ becomes less effective. Instead, it is more appropriate to use a scaled version ($\sqrt{n}V_n$) as the test statistic for larger sample sizes to improve accuracy and consistency across implementations. Despite this adjustment, the Kuiper test still has power and specificity issues. Thus, instead of the Kuiper test we recommended using the DTS (Difference of Two Samples) statistic, which calculates the reweighted Wasserstein difference between the cumulative distribution functions (CDFs) of two circular distributions.[42] The DTS statistic has demonstrated greater sensitivity and robustness when comparing both overall and clustered circular distributions.

## EXPECTED OUTCOMES

In this protocol, we implemented multilinear regression statistical methodology to detect and characterize the spatiotemporal dynamics of traveling waves in non-oscillatory neural activity. Following successful neural event and traveling wave detection, features of the traveling wave such as speed and direction can be estimated by the parameters of the fitted plane (Figure 8).

## LIMITATIONS

There is potential for misclassification of IEDs and bursts by using these methods. It is recommended to validate the IED detection algorithm's precision, by calculating the algorithm's positive predictive value against ratings of experienced epileptologists. Secondly, not all IEDs or seizures within the dataset fit the set model and may be used for analysis. Due to clinical limitations, the locus of the recording is limited to one area (the predicted SOZ location). The SOZ location is estimated prior to UMA placement, limiting the patient sample to those who have a predicted focalized seizure pattern. Additionally, due to the small size of the microelectrode array, recordings are obtained from a 4 by 4 mm patch of cortex limiting the area of brain sampled, potentially contributing to a selection bias. However, due to the microelectrode array's small size and placement in a homogenous brain area, detection and characterization of neural events and wave propagation are not susceptible to confounding effects of gyral anatomy.

## TROUBLESHOOTING

### Problem 1

Wave visualization does not reflect the presence or absence of a traveling wave, resulting in edge cases, where there may not be a traveling wave but when sorted the MUA firing looks like a traveling wave (steps 15,16).

### Potential solution

Traveling wave detection sensitivity is impacted by factors such as window size, signal rankings, and wave speed. A large window size may pick up unnecessary neural events that are not a part of the wave leading to poor plane fitting and false positives. A potential solution is to narrow the window size to isolate the wave and exclude unrelated events. There are two main ways to visualize traveling waves that emphasize either spatial or temporal information. Traveling waves can be visualized across space via electrode number, Figure 8D shows how a wave moves through the Utah array. This visualization approach provides an intuitive understanding of how the wave moves across the electrode array in space and captures the wavefront's direction and propagation speed across the

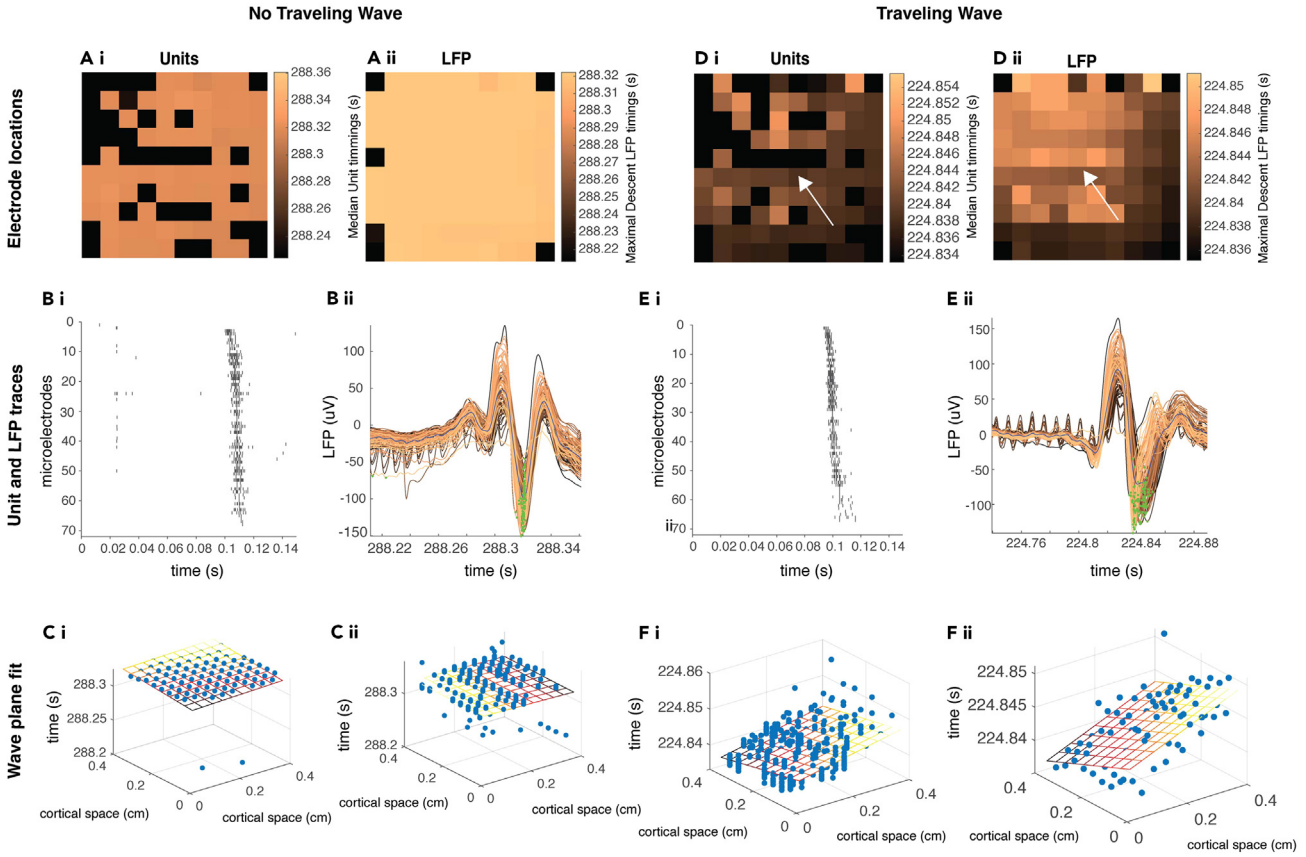


**Figure 8. Expected outcomes of traveling wave detection and characterization**

Two example anesthesia bursts demonstrating the absence and presence of a traveling wave respectively. **Top row:** Representative anesthesia bursts across each microelectrode superimposed on the footprint of the UMA. Colors represent the neural event timings of each electrode. Observe the sequential multiunit firing across the electrodes in (**Di**) indicating the presence of a traveling wave. White velocity vector shown on the UMA footprint indicates wave direction as it propagates across the microelectrodes. Contrast this to (**Ai**) where multiunit spikes occur simultaneously indicating the absence of a traveling wave. Similarly, observe the sequential LFP voltage minima timings across the electrodes in (**Dii**) indicating the presence of a traveling wave. Contrast this to (**Aii**) where LFP voltage minima timings occur simultaneously indicating the absence of a traveling wave. **Middle row:** Raster plots of multiunit firing and filtered LFP traces across microelectrodes as labeled in the top row. Observe that the MUA firing timings occur at successively later times across the electrodes in the traveling wave column (**Bi**) in contrast to the non-traveling wave column (**Ei**). The raster spike times are sorted by **median spike time** for each microelectrode during the specified burst window. LFP traces are ranked by voltage minima timings represented by the green-colored dots. Observe that the LFP voltage minima timings occur at successively later times across the electrodes in traveling wave (**Eii**) in contrast to the non-traveling wave (**Bii**). **Bottom row:** Spatiotemporal distribution of multiunit spikes and LFP voltage minima timings of the two example bursts. Fitted planes estimated from the multi-linear regression framework show the best fit between the neural event trimmings and the locations of the electrodes. Solid circles denote the neural event timings across the electrodes. Least squares linear regression was applied to recover its propagation axis and speed. Propagation axis is colored by activation sequence (blue to yellow). Observe the flat slope of the linear regression model in panel **Ci,ii** indicating the absence of a traveling wave in contrast to the large slope of the propagation axis in (**Fi,ii**) indicating the presence of a traveling wave. Features of the traveling wave such as speed and direction may be estimated by the parameters of the fitted plane.

grid. Additionally, traveling waves can be visualized by the order of signal rankings (MUA or LFP minima timings) or in oscillatory data, by the phase of oscillation. Visualizing waves via signal rankings provides a detailed temporal progression of wave activity by sorting electrodes by timing to reveal the sequence of activation. This visualization approach may falsely create an appearance of spatiotemporal order leading to false positives in traveling wave visualization; Figure 8B shows an example of such an edge case where the traveling wave in the LFP minima timings is visually not a traveling wave (Bii), however a traveling wave falsely appears in the neuronal firing (Bi). Combining spatial and temporal visualizations, such as through electrode-based maps and signal-ranking plots, can further reduce false positives and improve confidence in wave detection. If a traveling wave

propagates with a high speed across the electrode array, the temporal differences in the signal rankings between electrodes will be smaller which may lead to incorrect inferences about wave presence as temporal differences in signal rankings become indistinguishable from noise or random neural firing. For slow-propagating waves, the temporal differences are more pronounced, which can aid in detection. While slower waves may be more reliably detected they may require larger analysis window sizes, risking the inclusion of noise or unrelated activity. It is important to consider the balance between window size, signal rankings, and traveling wave speed to optimize traveling wave detection sensitivity and computational efficiency.

### Problem 2

Presence of broken or noisy channels across the UMA (step 7).

### Potential solution

It is still possible to detect waves despite a substantial number of broken electrodes. You may still be able to detect waves without recording from all 96 electrodes of the array. It is possible to measure waves across a smaller dimension of the array, for example Zhang et al. measured waves on a single-trial basis using a 3 × 8 electrode grid. Depending on your power analysis, a smaller electrode size may be sufficient to detect waves to investigate your research question.[12]

### Problem 3

Neural activity may lack a salient event, thereby not providing us a clear time envelope to apply traveling wave analyses (step 16).

### Potential solution

If lacking a specified time point, it is still feasible to measure traveling waves based on point estimators by applying the cross-correlation technique. This technique will allow us to detect waves in the cross-correlation between channels. Liou et al. validated cross correlation as a highly robust method to identify traveling waves without a salient neural event providing a specific time envelope to focus traveling waves analyses around.[3] Additionally, you can use generalized phase to detect the waves as an alternative wave classification methodology that is appropriate for detecting waves without a specific time point.[10]

### Problem 4

The traveling wave detection algorithm described is designed to detect planar waves, which may limit its ability to identify and characterize more complex wave patterns, such as spiral or rotating waves. This can result in incomplete analysis when these more intricate waveforms are present (step 17).

### Potential solution

The algorithm can be modified to detect and characterize complex wave patterns by incorporating techniques from vector calculus. Complex wave patterns have been detected in microelectrode arrays via vector calculus by taking the second derivative across two-dimensional space.[32]

### Problem 5

When working with large datasets, running analyses can be computationally demanding, leading to significantly longer processing times. This can become a bottleneck, especially when using complex models or algorithms that require substantial memory and processing power.

### Potential solution

To address this issue, it is recommended to utilize a computing cluster with multiple cores and larger RAM, enabling parallelization where applicable. By distributing the workload across multiple processors, parallelization can significantly reduce run time, making it more efficient to handle large-scale data analyses.

### Problem 6

The waves may not have a bimodal propagation, instead they may propagate multimodally such as in three different directions, therefore a different statistical methodology will need to be developed to quantitatively model the overall direction sub-distributions (step 22).

### Potential solution

To address this issue, a statistical framework such as implementing a clustering algorithm could help classify the observed wave directions into distinct groups, facilitating the analysis of the multimodal nature of the propagation. Statistical tests can then be applied to validate the significance of the identified modes and their interactions, providing a comprehensive understanding of the underlying wave dynamics.

## RESOURCE AVAILABILITY

### Lead contact

Further information and requests for resources should be directed to and will be fulfilled by the lead contact, Elliot H. Smith, PhD (e.h.smith@utah.edu).

### Technical contact

Questions about the technical specifics of performing the protocol should be directed to and will be answered by the technical contact, Veronica M. Zarr (veronica.zarr@utah.edu).

### Materials availability

This work did not produce novel reagents.

### Data and code availability

All analysis code is deposited to public repository GitHub, referenced in the key resources table.

Original data and analysis code have been deposited to Zenodo: https://doi.org/10.5281/zenodo.14889974, referenced in the key resources table.

## ACKNOWLEDGMENTS

We would like to thank the Schevon and Rolston labs for their support and contributions. This research received funding from various sources, including NIH NINDS R21 NS113031 (J.D.R.), NIH NINDS K23 NS114178 (J.D.R.), NIH S10 OD018211 (C.A.S.), NIH R01 NS084142 (C.A.S.), NIH NINDS 5T32 NS115723-04 (V.M.Z.), and a Junior Investigator Award from the American Epilepsy Society (E.H.S.).

## AUTHOR CONTRIBUTIONS

The initial draft of the manuscript was authored by V.M.Z., and E.H.S. conducted the review and editing of the manuscript.

## DECLARATION OF INTERESTS

The University of Utah maintains a financial interest in the company that manufactures Utah microelectrode arrays (Blackrock Neurotech). Additionally, J.D.R. reports personal fees from Medtronic, and G.M.M. reports personal fees from Koh Young Inc.

## REFERENCES

1. Smith, E.H., Liou, J.Y., Merricks, E.M., Davis, T., Thomson, K., Greger, B., House, P., Emerson, R.G., Goodman, R., McKhann, G.M., et al. (2022). Human interictal epileptiform discharges are bidirectional traveling waves echoing ictal discharges. Elife *11*, e73541. https://doi.org/10.7554/eLife.73541.

2. Muller, L., Chavane, F., Reynolds, J., and Sejnowski, T.J. (2018). Cortical travelling waves: mechanisms and computational principles. Nat. Rev. Neurosci. *19*, 255–268. https://doi.org/10.1038/nrn.2018.20.

3. Liou, J.Y., Smith, E.H., Bateman, L.M., McKhann, G.M., Goodman, R.R., Greger, B., Davis, T.S., Kellis, S.S., House, P.A., and Schevon, C.A. (2017). Multivariate regression methods for estimating velocity of ictal discharges from human microelectrode recordings. J. Neural. Eng. *14*, 044001.

4. Das, A., Zabeh, E., and Jacobs, J. (2022). How can we detect and analyze traveling waves in human brain oscillations?. Preprint at PsyArXiv. https://doi.org/10.31234/osf.io/jhnpr.

5. Smith, E.H., Liou, J.y., Davis, T.S., Merricks, E.M., Kellis, S.S., Weiss, S.A., Greger, B., House, P.A., McKhann II, G.M., Goodman, R.R., et al. (2016). The ictal wavefront is the spatiotemporal source of discharges during spontaneous human seizures. Nat. Commun. *7*, 11098.

6. Bhattacharya, S., Brincat, S.L., Lundqvist, M., and Miller, E.K. (2022). Traveling waves in the prefrontal cortex during working memory. PLoS Comput. Biol. *18*, e1009827. https://doi.org/10.1371/journal.pcbi.1009827.

7. Diamond, J.M., Diamond, B.E., Trotta, M.S., Dembny, K., Inati, S.K., and Zaghloul, K.A. (2021). Travelling waves reveal a dynamic seizure source in human focal epilepsy. Brain *144*, 1751–1763. https://doi.org/10.1093/brain/awab089.

8. Diamond, J.M., Withers, C.P., Chapeton, J.I., Rahman, S., Inati, S.K., and Zaghloul, K.A. (2023). Interictal discharges in the human brain are travelling waves arising from an epileptogenic source. Brain *146*, 1903–1915. https://doi.org/10.1093/brain/awad015.

9. Withers, C.P., Diamond, J.M., Yang, B., Snyder, K., Abdollahi, S., Sarlls, J., Chapeton, J.I., Theodore, W.H., Zaghloul, K.A., and Inati, S.K. (2023). Identifying sources of human interictal discharges with travelling wave and white matter propagation. Brain *146*, 5168–5181. https://doi.org/10.1093/brain/awad259.

10. Davis, Z.W., Muller, L., Martinez-Trujillo, J., Sejnowski, T., and Reynolds, J.H. (2020). Spontaneous travelling cortical waves gate perception in behaving primates. Nature *587*, 432–436. https://doi.org/10.1038/s41586-020-2802-y.

11. Zhang, H., and Jacobs, J. (2015). Traveling Theta Waves in the Human Hippocampus. J. Neurosci. *35*, 12477–12487. https://doi.org/10.1523/JNEUROSCI.5102-14.2015.

12. Zhang, H., Watrous, A.J., Patel, A., and Jacobs, J. (2018). Theta and Alpha Oscillations Are Traveling Waves in the Human Neocortex. Neuron *98*, 1269–1281.e4. https://doi.org/10.1016/j.neuron.2018.05.019.

13. Stern, M.A., Cole, E.R., Gross, R.E., and Berglund, K. (2024). Seizure event detection using intravital two-photon calcium imaging data. Neurophotonics *11*, 024202. https://doi.org/10.1117/1.NPh.11.2.024202.

14. House, P.A., MacDonald, J.D., Tresco, P.A., and Normann, R.A. (2006). Acute microelectrode array implantation into human neocortex: preliminary technique and histological considerations. Neurosurg. Focus *20*, E4. https://doi.org/10.3171/foc.2006.20.5.5.

15. Schevon, C.A., Weiss, S.A., McKhann, G., Goodman, R.R., Yuste, R., Emerson, R.G., and Trevelyan, A.J. (2012). Evidence of an inhibitory restraint of seizure activity in humans. Nat. Commun. *3*, 1060. https://doi.org/10.1038/ncomms2056.

16. Normann, R.A., and Fernandez, E. (2016). Clinical applications of penetrating neural interfaces and Utah Electrode Array technologies. J. Neural. Eng. *13*, 061003. https://doi.org/10.1088/1741-2560/13/6/061003.

17. Wang, Y., Yang, X., Zhang, X., Wang, Y., and Pei, W. (2023). Implantable intracortical microelectrodes: reviewing the present with a focus on the future. Microsyst. Nanoeng. *9*, 7–17. https://doi.org/10.1038/s41378-022-00451-6.

18. seizureCodes/find_inflections.m at master elliothsmith/seizureCodes GitHub. https://github.com/elliothsmith/seizureCodes/blob/master/find_inflections.m.

19. (2024). Psth. https://www.mathworks.com/matlabcentral/fileexchange/14745-psth.

20. smoothdata - Smooth noisy data - MATLAB. https://www.mathworks.com/help/matlab/ref/smoothdata.html.

21. Berens, P. (2009). CircStat: A MATLAB Toolbox for Circular Statistics. J. Stat. Softw. *31*, 1–21. https://doi.org/10.18637/jss.v031.i10.

22. Schymura, C. (2016). mvmdist, version 9b28bf0 (GitHub).

23. Cloherty, S. (2020). hermans-rasson, version ceef2c4 (GitHub).

24. Mercier, M.R., Dubarry, A.-S., Tadel, F., Avanzini, P., Axmacher, N., Cellier, D., Vecchio, M.D., Hamilton, L.S., Hermes, D., Kahana, M.J., et al. (2022). Advances in human intracranial electroencephalography research, guidelines and good practices. Neuroimage *260*, 119438. https://doi.org/10.1016/j.neuroimage.2022.119438.

25. Hanrahan, S.J., Greger, B., Parker, R.A., Ogura, T., Obara, S., Egan, T.D., and House, P.A. (2013). The effects of propofol on local field potential spectra, action potential firing rate, and their temporal relationship in humans and felines. Front. Hum. Neurosci. *7*, 136. https://doi.org/10.3389/fnhum.2013.00136.

26. Campbell, J.M., Davis, T.S., Anderson, D.N., Arain, A., Davis, Z., Inman, C.S., Smith, E.H., and Rolston, J.D. (2024). Macroscale traveling waves evoked by single-pulse stimulation of the human brain. Preprint at bioRxiv. https://doi.org/10.1101/2023.03.27.534002.

27. Find local maxima - MATLAB findpeaks. https://www.mathworks.com/help/signal/ref/findpeaks.html.

28. Kutner, M.H., Nachtsheim, C., and Neter, J. (2004). In Applied Linear Regression Models., Fourth, M.A. Boston, ed. (McGraw-Hill/Irwin), p. 701.

29. Buzsáki, G., and Draguhn, A. (2004). Neuronal Oscillations in Cortical Networks. Science *304*, 1926–1929. https://doi.org/10.1126/science.1099745.

30. Massimini, M., Huber, R., Ferrarelli, F., Hill, S., and Tononi, G. (2004). The sleep slow oscillation as a traveling wave. J. Neurosci. *24*, 6862–6870. https://doi.org/10.1523/JNEUROSCI.1318-04.2004.

31. Muller, L., Piantoni, G., Koller, D., Cash, S.S., Halgren, E., and Sejnowski, T.J. (2016). Rotating waves during human sleep spindles organize global patterns of activity that repeat precisely through the night. Elife *5*, e17267. https://doi.org/10.7554/eLife.17267.

32. Liou, J.Y., Smith, E.H., Bateman, L.M., Bruce, S.L., McKhann, G.M., Goodman, R.R., Emerson, R.G., Schevon, C.A., and Abbott, L.F. (2020). A model for focal seizure onset, propagation, evolution, and progression. Elife *9*, e50927.

33. Martinet, L.-E., Fiddyment, G., Madsen, J.R., Eskandar, E.N., Truccolo, W., Eden, U.T., Cash, S.S., and Kramer, M.A. (2017). Human seizures couple across spatial scales through travelling wave dynamics. Nat. Commun. *8*, 14896. https://doi.org/10.1038/ncomms14896.

34. Alamia, A., Timmermann, C., Nutt, D.J., VanRullen, R., and Carhart-Harris, R.L. (2020). DMT alters cortical travelling waves. Elife *9*, e59784. https://doi.org/10.7554/eLife.59784.

35. Aggarwal, A., Brennan, C., Luo, J., Chung, H., Contreras, D., Kelz, M.B., and Proekt, A. (2022). Visual evoked feedforward–feedback traveling waves organize neural activity across the cortical hierarchy in mice. Nat. Commun. *13*, 4754. https://doi.org/10.1038/s41467-022-32378-x.

36. Aggarwal, A., Luo, J., Chung, H., Contreras, D., Kelz, M.B., and Proekt, A. (2024). Neural assemblies coordinated by cortical waves are associated with waking and hallucinatory brain states. Cell Rep. *43*, 114017. https://doi.org/10.1016/j.celrep.2024.114017.

37. Zhang, H., Watrous, A.J., Patel, A., and Jacobs, J. (2017). Theta and alpha oscillations are traveling waves in the human neocortex. Neuron *98*, 1269–1281. https://doi.org/10.1101/218198.

38. Rubino, D., Robbins, K.A., and Hatsopoulos, N.G. (2006). Propagating waves mediate information transfer in the motor cortex. Nat. Neurosci. *9*, 1549–1557. https://doi.org/10.1038/nn1802.

39. Kleen, J.K., Chung, J.E., Sellers, K.K., Zhou, J., Triplett, M., Lee, K., Tooker, A., Haque, R., and Chang, E.F. (2021). Bidirectional propagation of low frequency oscillations over the human hippocampal surface. Nat. Commun. *12*, 2764. https://doi.org/10.1038/s41467-021-22850-5.

40. Sato, T.K., Nauhaus, I., and Carandini, M. (2012). Traveling Waves in Visual Cortex. Neuron *75*, 218–229. https://doi.org/10.1016/j.neuron.2012.06.029.

41. Davis, Z.W., Benigno, G.B., Fletterman, C., Desbordes, T., Steward, C., Sejnowski, T.J., H. Reynolds, J., and Muller, L. (2021). Spontaneous traveling waves naturally emerge from horizontal fiber time delays and travel through locally asynchronous-irregular states. Nat. Commun. *12*, 6057. https://doi.org/10.1038/s41467-021-26175-1.

42. DTS Test — two_sample https://twosampletest.com/reference/two_sample.html.